Title	Novel digital compensation approaches for envelope tracking amplifiers
Author(s)	Hekkala, Atso; Kotelba, Adrian; Lasanen, Mika; Järvensivu, Pertti; Mämmelä, Aarne
Citation	Wireless Personal Communications. Springer. Vol. 62 (2012) No: 1, Pages 55 - 77
Date	2012
URL	http://dx.doi.org/10.1007/s11277-010-0038-0
Rights	Post-print version of the article. The final publication is available at link.springer.com. This article may be downloaded for personal use only.

Novel Digital Compensation Approaches for Envelope Tracking Amplifiers

Atso Hekkala, Adrian Kotelba, Mika Lasanen, Pertti Järvensivu, and Aarne Mämmelä

VTT Technical Research Centre of Finland, P.O. Box 1100, FI-90571 Oulu, Finland

atso.hekkala@vtt.fi

Parts of this paper were presented at the IEEE International Symposium on Spread Spectrum Technologies and Application, Bologna, Italy, August, 2008 and at the IEEE Personal, Indoor, and Mobile Communication Symposium, Cannes, France, September, 2008.

This paper considers the compensation of the envelope tracking (ET) amplifier. In particular, we propose a new predistortion architecture for the ET amplifier. In addition, we develop new algorithms for time misalignment compensation between the input signals of the ET amplifier and compare the methods to a previously presented method. Our results indicate that using the proposed architecture with optimal predistorter, we achieve over 40 dB better adjacent channel power than using a previously presented architecture. In addition, the time misalignment compensation methods give very accurate timing estimates. The time misalignment compensation with the predistortion reduces spectral regrowth due to the nonlinear ET amplifier and improves the power efficiency of the ET amplifier.

Adaptive compensation; polynomial predistorter; predistorter architecture; time misalignment

Introduction

The trend in wireless communication shows an ever increasing need for higher data rates. This requires exploiting advanced modulation techniques, such as wideband code division multiple access (WCDMA) or orthogonal frequency division multiplexing (OFDM), where both the phase and the amplitude of the signal carry information. These systems are very sensitive to the distortions introduced by the transmitter's analog parts.

High power amplifier (HPA) is a critical component in the transmitter due to the tradeoff between its linearity and efficiency. As a modification of the envelope elimination and restoration structure [1] the envelope tracking (ET) amplifier [2] has been seen as one of the most promising power efficient structures. However, the ET structure has a few severe drawbacks, e.g. sensitivity to time misalignment

of RF and envelope signals as well as nonlinearity due to changing supply voltage [3, 4].

Predistortion has been found as a suitable technique for linearizing the HPA [5, 6]. Due to the two-input single-output structure of the ET amplifier, the predistorter architecture has to be carefully designed. A state-of-the-art predistorter architecture for the ET amplifier has been presented in [4]. We find out that the state-of-the-art method of predistorting the ET amplifier is not necessarily a generic approach, and as such, is not guaranteed to work with all ET amplifiers.

In addition to nonlinearity, one of the most serious problems with envelope-tracking amplifiers is the need to accurately align in time the two input signals, i.e., a modulated RF signal and a signal which carries its envelope. A precise alignment is required because the final transistor of an envelope-tracking amplifier is typically supplied with just the minimum supply voltage needed to prevent it from saturating, given the instantaneous value of the amplitude component of RF signal [7]. Consequently, if the input signals are not properly aligned in time, the supply voltage could be greater than the required reducing the power efficiency. If the supply voltage is smaller than the required, it causes clipping of the output signal due to saturation of the amplifier. The time misalignment compensation in the ET structure has been studied in [4]. The authors propose to use cross-covariance and phase comparison to estimate the time misalignment. The approach is based on a one-shot method and, in addition, it cannot necessarily be applied because of their assumptions on an ideal predistorter and an amplifier model without phase distortion.

In this paper, we propose a general predistorter approach, which can be applied to a wide class of ET amplifiers. We analyze and compare it against the state-of-the-art architecture. Furthermore, using the proposed architecture, we demonstrate the performance of the optimal as well as adaptive predistorters for the linear filters and the ET amplifier. We also discuss the complexity of the adaptive predistorters.

In addition, we analyze and further develop the time misalignment compensation methods presented originally in [4]. Furthermore, we propose a novel time misalignment compensation method. We demonstrate in a detailed manner the

performance of the time misalignment compensation methods for linear filters and the ET amplifier with optimal as well as adaptive predistorters.

Parts of this paper were presented in our earlier conference papers [8–10]. In this combined paper, we give a revised and unified presentation of the earlier work. We create a more comprehensive presentation of digital compensation approaches. Moreover, an extensive comparison of the methods is enabled by additional simulation examples.

The rest of the paper is organized as follows. In Section II, we present the system model. Then we discuss predistorter architectures in Section III. In Section IV, we present the time misalignment compensation approach. In Section V, we show some simulation results. Finally, Section VI draws the conclusion of the paper.

System description

Simplified system model

We present the simplified block diagram of the system model in Fig. 1. The system model is based on a WCDMA base station transmitter. The transmitter is modeled using a complex baseband model. The actual transmitter model consists of a signal source, linear filters, and a high power amplifier. In addition to these, we introduce a digital predistorter block to compensate the time misalignments and distortions introduced by the analog parts of the transmitter. The adaptive controller calculates the parameters of the digital compensator by comparing the HPA output signal z and the reference signal r. The reference model block is a delay block with delay τ. Symbols T_{env}, T_{rf}, and T_{fb} represent delays introduced in envelope, RF, and feedback branches, respectively.

The tunable delay filters, needed for the time misalignment compensation, are allpass fractional-delay filters implemented as infinite-impulse response (IIR) gathering structures with Thiran approximation [11]. In our case, the order of the filters is 20 and the approximation order is 3.

We measure the analog parts of the transmitter and model them into the digital domain using a sampling frequency of 76.8 MHz. A dual carrier WCDMA signal is used as an input signal u, i.e., no special training signal is used. When constructing the signal model, we follow closely the 3rd Generation Partnership Project (3GPP) specifications [12]. Crest factor reduction is applied to the

generated signal. We assume that undersampling is used in the feedback branch, limiting the useful bandwidth of the forward branch to 38.4 MHz, as in [13]. In our system model, the target gain g for the predistorted amplifier is 13 dB. Time misalignments and adjacent channel powers (ACPs) are used as performance measures. In the next subsections, we introduce briefly the models we used for the linear filters and ET amplifier.

Linear filters

We model the linear filters using measurements carried out on real analog RF filters. We use the direct-design method in the frequency domain [14] to model them as stable and nonminimum-phase IIR filters with the following transfer function

$$H(z) = \frac{a_0 + a_1 z^{-1} + ... + a_5 z^{-5}}{1 + b_1 z^{-1} + ... + b_6 z^{-6}}$$

where a_0 = 0.0329-j0.0236, a_1 = -0.1933+j0.2085, a_2 = -1.0722+j0.6911, a_3 = -1.3787+j0.1907, a_4 = -0.5342-j0.6205, a_5 = -0.0005-j0.3532, b_1 = -1.4587+j0.5565, b_2 = 0.3035+j0.9324, b_3 = -0.1959+j0.4437, b_4 = -0.0747+j0.0713, b_5 = -0.0241-j0.0096, and b_6 = 0.0149-j0.0140.

Envelope tracking amplifier

The ET amplifier can be thought as a nonlinear two-input single-output system. The input signals to the amplifier are the RF signal x and the baseband envelope signal e (see Fig. 1). The output signal of the amplifier is the RF signal z. Consequently, one can represent the nonlinear ET amplifier with a nonlinear complex mapping $z = F(e, x)$ where $e = |x|$. The amplitude-to-amplitude (AM/AM) and amplitude-to-phase (AM/PM) characteristics are sufficient to describe the nonlinear complex mapping F without memory.

We characterize the envelope tracking amplifier model using measurements on a real lateral double-diffused MOSFET (LDMOS) amplifier. We obtain the AM/AM) and the AM/PM characteristics for a number of drain supply voltages V_{dd}. We build a quasi-memoryless parametric model of the amplifier using the following nonlinear functions

$$h(A) = \frac{(g_0 + g_1 A)A}{\sqrt[s]{1 + [(g_0 + g_1 A)A/L]^s}}$$
$$\Phi(A) = \arctan\left[a \exp(bA)(A - p)^2 + q\right]$$

to model the AM/AM and AM/PM characteristics of the ET amplifier. The symbol A represents the input signal amplitude. The parameters g_0, g_1, L, s, a, b, p, and q are found by a small-scale nonlinear least squares fit to the measurement data. These parameter values depend on V_{dd} and are summarized in Table 1. The parameters for other supply voltages are obtained by linear interpolation.
The AM/AM and AM/PM characteristics for different V_{dd} values are shown in Figs. 2 and 3. Measurement data are shown as well. The V_{dd} is almost linearly proportional to the amplitude of the envelope signal, e.g. when input powers are 32.8 dBm and 38.6 dBm, the V_{dd} values are 15 V and 30 V, respectively. However, we assume that there is a minimum drain supply voltage V_{min} = 3 V that must be maintained to keep the amplifier operational. The fixing of V_{dd} makes the AM/AM and AM/PM curves piecewise smooth, i.e., there is no first order derivative at the point where V_{dd} starts to raise.
Using the parametric model, we obtain the nominal curves for AM/AM and AM/PM characteristics, i.e. nominal mapping $z = F(|x|, x)$, with dynamically varying V_{dd}, see dashed lines in Figs. 2 and 3.

Predistortion architecture

The digital predistorter presented in Fig. 1 can be separated into linear and nonlinear predistorters, see our proposal e.g. in Fig. 5. The linear predistorter is introduced to compensate the linear filters. The nonlinear predistorter compensates the nonlinearities of the amplifier itself.

Linear predistortion

It is intuitively understandable that the linear predistorter must be in the RF branch because the linear filters are in RF branch. The linear predistorter compensates the magnitude and phase responses of the linear filters such that the combined response of the linear filters and predistorter follows the response of the reference model. The signals in the RF and envelope branches are time aligned by introducing a fixed delay block in the envelope branch. The group delay of this block equals to the group delay of the reference model.

The linear predistorter is implemented using a 63–tap finite impulse response (FIR) filter. An optimal solution is obtained by the direct-design method in the frequency domain [14]. For an adaptive solution, the constrained LMS-algorithm is used to obtain the filter coefficients of the predistorter. An adaptive inverse control technique [15] is used for training the predistorter.
The bandwidth of the feedback branch is limited to 38.4 MHz. Thus, in order to keep the response of the linear predistorter constant for frequencies higher than 19.2 MHz, constraints are introduced at those frequencies. For more discussions on the linear predistorter, see [16].

Nonlinear predistortion

In general, the predistorter should implement a complex and nonlinear mapping G such that the output signal z is a delayed copy of u, i.e., $z(n) = gu(n\text{-}\tau)$.
In [4], the authors propose to place a nonlinear predistorter only in the RF branch, see Fig. 4. For mathematical simplifications in the analysis of the predistortion structure, we assume the linear predistorter to be ideal, i.e., $x(n) = v(n\text{-}\tau)$. The adaptive predistortion structure implements the mapping G such that

$$z(n) = F\left[e(n), x(n)\right] = F\left[\left|u(n-\tau)\right|, G\left[u(n-\tau)\right]\right] = gu(n-\tau).$$

The desired mapping $G(u)$ can be found by discretizing the problem. More precisely, we assume that the dynamic range of the input signal u is divided into I regions and a sample u_i represents the ith region. The mapping $G(u)$ is then found by solving a set of I nonlinear equations

$$F\left[\left|u_i(n)\right|, G\left[u_i(n)\right]\right] = gu_i(n), \quad i = 1,2...,I$$

The mapping $G(u)$ is given in a discrete form as a set of i nodes $G(u_i)$. In the envelope tracking amplifier, the power level of the input RF signal cannot exceed a certain value, which is in our case 38.6 dBm. Therefore, the mapping $G(u_i)$ cannot be arbitrary and the set of nonlinear equations (4) should be solved subject to the additional constraint

$$\left|G\left[u_k(n)\right]\right| \le v_{\max} = \sqrt{2} \cdot 10^{\frac{38.6-30}{20}}$$

where $v_{\max}$ represents a maximum allowed amplifier input signal level. The problem of solving (4) subject to (5) is analytically intractable. Therefore, the solution must be found by numerical methods.

Since the predistorter affects only the input signal x and the envelope signal e remains unaffected, there is a possibility that the amplifier cannot provide sufficient gain to achieve the target gain g, 13 dB. For example, if the input power is 20 dBm, then V_{dd} is 3 volts and the amplifier provides about 6 dB gain, see Fig. 2. Thus, the predistorter needs to increase the amplifier input power at least to 27 dBm to meet the requirement. However, for this input power the amplifier provides even less gain, which requires even further increase of the input power. The process will continue until the maximum input power level is reached. Consequently, we cannot achieve the target gain because the amplifier does not provide sufficient gain at this level of V_{dd}.

To solve the possible problem of insufficient gain, we propose the adaptive control structure where predistorter affects both the RF and the envelope branches shown in Fig. 5. To simplify the analyses of the predistorter structure, we assume that the linear predistorter is ideal, i.e., $x(n) = v(n-\tau)$. The optimization algorithm tries to find a mapping G such that $z(n) = F[e(n), x(n)] = F[|G[u(n-\tau)]|, G[u(n-\tau)]] = gu(n-\tau)$, which is different from (3).

By defining a new nonlinear mapping $H[u(n)] = g^{-1}F[|u(n)|, u(n)]$, we obtain

$$\begin{aligned} g^{-1}z(n) &= g^{-1}F\left[\left|G\left[u(n-\tau)\right]\right|, G\left[u(n-\tau)\right]\right] \\ &= H\left[G\left[u(n-\tau)\right]\right] = u(n-\tau) \end{aligned}$$

which implies that $G(\cdot)$ is the inverse function of $H(\cdot)$. In other words, the optimal predistorter varies the source signal to the ET amplifier x and, indirectly, the envelope signal e. Consequently, the AM/AM and AM/PM characteristics remain the same, i.e., the nominal ones, due to a fixed relationship between x and e. To the nonlinear predistorter, the ET amplifier appears to be a nonlinear single-input single-output system. Thus, it can be compensated with any predistorter [17]. Using the AM/AM and AM/PM characteristics of the ET amplifier, the optimal solution for the predistorter is obtained by a look-up-table (LUT) based nonlinear predistorter. Optimal LUT based nonlinear predistorter is used in analysis and simulations of predistorter architectures and as a reference for the performance tests with an adaptive predistorter.

For adaptive compensation of the ET amplifier model, we use a polynomial predistorter structure. The polynomial predistorter output v can be given by [17]

$$v(n) = \sum_{k=1}^{K} a_k u(n)\left|u(n)\right|^{k-1}$$

where u is the predistorter input, K is the order of the predistorter, and a_k is the polynomial coefficient.

In this work, the adaptive identification of the nonlinear predistorter is done using the indirect learning architecture [17], which is a form of nonlinear adaptive inverse control. In the indirect learning architecture, the predistorter-training block, i.e. the postdistorter, is driven by the ET amplifier output z. In order to achieve the inverse of the ET amplifier, the block adjusts its parameters using an adaptive optimization algorithm. After convergence, the inverse model is directly used as the nonlinear predistorter.

The predistorter coefficients a_k are found by solving a least squares (LS) problem [17]. To obtain a_k in (7), we use either direct matrix inversion in the LS method or recursive least squares (RLS) method presented in [17] and [18], respectively.

Time misalignment compensation

To compensate the time misalignment, we need to know both the RF and the envelope delays (T_{rf} and T_{env}) or the difference between them. We assume that we can use the phases and amplitudes separately for the compensation. We note that in the ideal case the envelope signal does not affect the phase of the output signal. This can be explained as follows. From Fig. 3, it can be seen that the change of the output phase with respect to the change of the supply voltage V_{dd} is about 2 degrees per volt. The change of the output signal due to the change of the envelope signal is small because the envelope signal and its delayed version are highly correlated. In particular, the correlation coefficient is greater than 0.9 for delays in the range of ±1 sample. In other words, the V_{dd} does not change significantly when envelope signal is delayed by one sample. Thus, we conclude that the change of the output signal phase is mainly caused by the input signal phase.

The amplitude is affected by both the envelope and RF delays. An exception is a case in which the envelope path is kept constant, i.e. when the amplitudes are small; see Fig. 2.

State-of-the-Art Method

The cross-covariance method for estimation of time misalignment between the RF and envelope signals in the envelope tracking amplifier is proposed in [2]. Our

structure slightly differs from the one presented in [2] in a sense that we delay the reference signal r rather than advance the feedback signal z.

The time misalignment between the envelope and RF paths is compensated as follows. First, the cross-covariance function of amplitudes of reference signal $A_r = |r|$ and feedback signal $A_z = |z|$ is calculated, i.e.,

$$R_{rz}(\tau) = \frac{1}{N}\sum_{n=1}^{N}\left[A_r(n) - \bar{A}_r\right]\left[A_z(n-\tau) - \bar{A}_z\right]$$

where τ denotes a time-lag which could be a fractional part of the sampling interval T_s. The symbols $\bar{A}_r$ and $\bar{A}_z$ denote, respectively, the average of A_r and A_z. The means are calculated over N samples. The time-lag t_c for which the cross-covariance function $R_{rz}(\tau)$ achieves its maximum is calculated and the tunable delay t_{pl} is set to t_c. Next, the phase error between the samples of the feedback signal $z(n)$ and a delayed source signal $r(n-t_{\mathrm{pl}})$ is calculated, i.e. $e(n) = \arg[r(n-t_{\mathrm{pl}})] - \arg[z(n)]$. The tunable delay t_{pl} is then adjusted such that the root-mean square of the phase error is minimized, i.e.,

$$t_{\mathrm{pl}} = \arg\min_{t_{\mathrm{pl}}} \sqrt{\frac{1}{N-1}\sum_{n=1}^{N}\left[e(n) - \bar{e}\right]^2}$$

where $\bar{e}$ denotes the average of $e(n)$ which is calculated over N samples. The time misalignment between the envelope and RF paths is approximately $T_{\mathrm{rf}} - T_{\mathrm{env}} \approx 2t_{\mathrm{pl}}$ for any envelope tracking amplifier [2]. Therefore, the additional delay to be applied in the envelope path is $t_{\mathrm{env}} \approx 2t_{\mathrm{pl}}$.

Model Reference Control method

The basic idea of model reference control is to adapt the controller in such a way that the overall response best matches the reference model response [19, p. 294]. Therefore, the time alignment of signals in envelope and RF paths can be achieved by setting t_{env} and t_{rf} such that the feedback signal $z(n)$ follows the delayed version of source signal $r(n) = s(n-t)$ where t is a reference delay. In other words, we adapt t_{env} and t_{rf} such that the overall response of time misalignment compensator and the nonlinear system matches the response of the reference model.

A block diagram of the time misalignment compensator which uses the average squared difference between feedback signal $z(n)$ and reference signal $r(n)$

$$F(t_{\mathrm{env}}, t_{\mathrm{rf}}) = \frac{1}{N}\sum_{n=1}^{N}\left|z(n) - r(n)\right|^2$$

as the cost function is shown in Fig. 6. The optimal values of t_{env} and t_{rf} correspond to the global minimum of (10).

Using a general steepest descent algorithm for minimization of (10), the partial derivatives of the cost function $\partial F/\partial t_{\mathrm{env}}$ and $\partial F/\partial t_{\mathrm{rf}}$ are difficult to estimate. Therefore, we use a derivative-free method with cyclic coordinate descent method [20, p. 227]. The optimization algorithm searches for the minimum of the cost function F cyclically with respect to the coordinate variables t_{env} and t_{rf}. For example, in the i_{th} iteration

$$t_{\mathrm{env}}^{i+1} = \arg\min_{t_{\mathrm{env}}} F\left(t_{\mathrm{env}}^{i}, t_{\mathrm{rf}}^{i}\right)$$

and in the (i+1)th iteration

$$t_{\mathrm{rf}}^{i+2} = \arg\min_{t_{\mathrm{rf}}} F\left(t_{\mathrm{env}}^{(i+1)}, t_{\mathrm{rf}}^{(i+1)}\right)$$

The process is then repeated starting with t_{env} again in the (i+2)th iteration and t_{rf} in the (i+3)th iteration.

In (11) and (12) one needs to estimate the minimum of $F(t_{\mathrm{env}}, t_{\mathrm{rf}})$ on a given line with respect to t_{env} or t_{rf}, respectively. In both cases, we measure $F(t_{\mathrm{env}}, t_{\mathrm{rf}})$ for three different delays (t_1, t_2, t_3) and use the inverse parabolic interpolation to estimate the delay t_4 for which (11) or (12) achieves its minimum [20, p. 200]. In particular, if t_1, t_2, and t_3 are additional delays and F_1, F_2, and F_3 are corresponding values of the cost function, the abscissa of the minimum point of the parabola is [20, p. 206]

$$t_4 = \frac{1}{2}\frac{b_{23}F_1 + b_{31}F_2 + b_{12}F_3}{a_{23}F_1 + a_{31}F_2 + a_{12}F_3}$$

where $a_{ij} = t_i - t_j$ and $b_{ij} = t_i^2 - t_j^2$.

Visible Delay of Phases and Cross-Covariance of Amplitudes Methods

We notice by measurements that we are able to see the phase difference between the ET amplifier input and output signals. Assuming the phase difference is coming only due to delays in the RF and feedback branches, we obtain a delay estimate TL for the visible delay of phases (VDP) method [4]

$$T_L = T_{\mathrm{rf}} + T_{\mathrm{fb}}$$

We use the similar right triangle geometry to calculate T_L. After some manipulations, we find the equation

$$T_L = \frac{\phi_i(l) - \phi_o(l)}{\phi_i(l) - \phi_i(l-1)}$$

where l is the timing index going through all the vector elements, and ϕ_i and ϕ_o are the phases of the ideal and feedback signal vectors. Fig. 7 clarifies the calculation of T_L. In order to exploit the similar right triangles, we need to select the indices l in (15) with the following criteria

$$\begin{aligned} l \quad = \quad & \{i; |\Delta\phi_i| > 0.2, |\phi_o - \phi_i| < 1, |\Delta\phi_i| < 1.5, \ldots \\ & |\Delta\phi_o| < 1.5, 0.9 < \Delta\phi_o / \Delta\phi_i < 1.1, |u| > 0.125\} \end{aligned}$$

where ϕ_i and ϕ_o are the phases of the ideal and feedback signals in radians, $\Delta\phi_i$ and $\Delta\phi_o$ model the derivates of the phases of the ideal and feedback signals, and u is the ideal signal with the maximum amplitude normalized to one. The conditions try to select the phases, which are quite similar in terms of the actual values and derivatives. In addition, it is essential to keep the absolute value of the derivates within a certain range when using the similar right triangle geometry. Moreover, the small amplitudes are restricted because the noise and the uncertainty of the predistorter have a large impact to the phase when the amplitudes are small. Finally, averaging of T_L in (15) is performed over the indices selected according to (16).

We notice that by using the signal amplitudes we can obtain a combined estimate of all delays T_C [4]

$$T_C = (T_{\mathrm{rf}} + T_{\mathrm{env}})/2 + T_{\mathrm{fb}}$$

We exploit cross-covariance of amplitudes (CCA) to get an estimate of T_C. The CCA function between input and output is given by [4]

$$R_{uz}(t) = \frac{1}{N}\sum_{i=1}^{N}\left\{|u(i)| - \frac{1}{N}\sum_{j=1}^{N}|u(j)|\right\}\left\{|z(i-t)| - \frac{1}{N}\sum_{j=1}^{N}|z(j)|\right\}$$

To estimate subsample accuracy for the maximum correlation point, we use a quadratic approximation, which is defined as [21]

$$T_{\mathrm{C}} = \frac{1}{2}\frac{R_{uz}(t_m+1) - R_{uz}(t_m-1)}{R_{uz}(t_m+1) - 2R_{uz}(t_m) + R_{uz}(t_m-1)} - t_m$$

where t_m is the time lag where the cross-covariance function $R_{uz}(t)$ achieves its maximum.

With the delays T_L and T_C, it is possible to approximate delay difference

$$T_{env} - T_{rf} = 2(T_C - T_L)$$

Equation (20) is basically the same as (36) in [4]. This approach could ideally be used in a one-shot way. However, we assume that accurate estimation in one shot may not be possible if preliminary errors are large. In addition, both T_C and T_L require their own estimations meaning that both estimation errors cumulate to the end result.

Another approach could be to first adapt RF + feedback delay near to zero and then start to track the envelope delay. In this case, an adaptive linear predistorter could be employed to obtain RF + feedback delay synchronization. Originally, the linear predistorter has been developed to compensate linear filters. In addition to that, it can handle all the delays in the RF and feedback branches by adjusting the group delay of the branches to a certain value, i.e., the group delay of the reference model. Together with the adaptive linear predistorter and e.g. the CCA method, we are able to compensate time mismatches between RF and envelope signals.

Results

Optimal predistortion

In the simulations with the optimal nonlinear predistorter, we ignore the linear predistorter and linear filters to simplify the simulation model. We use about 8000 signal samples as an input for each iteration cycle.

The gains versus input powers of the envelope tracking amplifier and the optimal predistorter using the state-of-the-art and the proposed architectures are shown in Figs. 8(a) and 8(b), respectively. The results suggest that the predistorter using the state-of-the-art architecture cannot completely compensate the amplifier nonlinearity. In other words, for the ET amplifier under study there is no mapping $G(u)$ such that (3) is satisfied with respect to the constraint (5). However, with the proposed architecture we are able to compensate completely the nonlinear behavior of the amplifier.

Fig. 9 shows the signal spectra at the output of the predistorted ET amplifiers using the state-of-the-art and the proposed architectures. Using the proposed architecture with the optimal predistorter, we achieve over 40 dB better ACPs.

In Fig. 10, we show the histograms of the timing estimate errors using the VDP and CCA methods. The RF and envelope delays are random variables with a uniform distribution between zero and one samples. The feedback delay is set to zero.

Fig. 10 (a) shows the RF + feedback delay estimation errors of the VDP method. Almost all of the estimations give better than 0.015 samples accuracy. In Fig. 10 (b), we present timing estimate errors of the CCA method. The accuracy of the CCA method is a bit worse than that of the VDP method. The CCA method gives a combined delay estimates, just according to (17). The CCA method works well also without predistorter whereas the VDP method does not. The VDP method suffers from the phase distortion of the uncompensated amplifier. In addition, the phase noise can degrade, or even collapse, the performance of the VDP method. Accurate oscillators or a phase noise compensation is clearly needed in the real implementation.

Considering Figs. 10 (c) – (f), we can also see the performance of joint delay estimation of CCA and VDP methods. In the joint estimation, we can compensate the time mismatch between RF and envelope branches. We update delay compensation blocks in RF and envelope branches after each iteration according to (20). In addition to the delay difference compensation, using (14), we force the RF + feedback delay to zero. Within three iterations, we achieve very accurate timing estimates. However, with more iterations even better performance is attained.

We show also cumulative density functions (CDFs) for ACPs using the joint delay estimation in Fig. 11. After three iterations, we achieve with 90 percent probability less than 10 dB loss of ACP comparing to the input signal ACP, i.e. -88 dB. Also within two iterations, we get quite good ACPs: almost all the time below -70 dB. Using optimal predistortion with optimal time misalignment compensation, we achieve also the -88 dB level of ACP. In the figures, ACPs are the mean values of lower and higher ACPs in decibels relative to the carrier power.

For comparison purposes, we model the time misalignment estimator presented in [4]. That estimator is assumed to be a one-shot method. Therefore, we can compare that estimator to the proposed method after one iteration. In Fig. 11, we can see that the proposed method gives roughly 10 dB better ACPs. The complexities of the both estimators are roughly at the same level.

We change the feedback delay to 0.66 samples and repeat the previous simulations. Comparing Figs. 10 and 12, we can say that the proposed methods work well also with the additional feedback delay: the timing estimate accuracies are at the same level as in Fig. 10 or only a slightly worse. This is the expected result from (20).

Using the model reference control method, a contour plot of the cost function (10) and achievable values of ACP after subsequent iterations are shown in Fig. 13. The reference delay equals $t = 6T_s$ and delays in RF and envelope paths are, respectively, $T_{rf} = 4.1744T_s$ and $T_{env} = 0.7821T_s$. The convergence of coordinate descent method to the optimal solution is illustrated in Fig. 13 by showing with bold line the direction of search, subsequent estimates of the pair (t_{env}, t_{rf}), and the value of ACP after each iteration.

Adaptive predistortion

In the simulations with adaptive predistorters, we first use calibration or acquisition of linear filters. In order to keep the ET amplifier as linear as possible in the acquisition, a downscaled signal level is used, i.e. the drain supply voltage remains constant. After the acquisition, i.e. in tracking phase, we train the delay estimation, nonlinear and linear predistorters one after another. To train the predistorters in each iteration, the signal block with 8000 samples is used. Physical and temporal orders of the predistortion are discussed more by the authors in [16].

Often, only odd order terms of K are used in polynomial predistorters [17]. Instead of that, here we use also even order terms due to high nonlinearity of the ET amplifier. The effects of the even order nonlinear terms have been studied earlier in [22]. In the simulations, the adaptive predistorter algorithms are converged after two iterations in the tracking phase. In the figures, ACP LO and ACP HI correspond to ACP of lower and higher adjacent bands in decibels relative to the carrier power.

In Fig. 14, we show the ACPs at the output of the ET amplifier with polynomial based adaptive predistorter and ideal time misalignment compensation. Only the 9th order predistorter achieves the ACP of -60 dB. The polynomial predistorter suffers from the piecewise smoothness of the AM/AM and AM/PM characteristics of the ET amplifier. We suspect that increasing the polynomial order we achieve a better performance. We can see the performance of the LS solution in Fig. 14 (d) and compare it to the corresponding RLS algorithm in Fig. 14 (b). The ACPs are the same. In general, the nonlinear predistorter seems to be a bottleneck for the lower ACPs.

The high complexity is one of the main problems of the RLS algorithm and the RLS with the nonlinearity order of 9 appears to be too complex for practical systems. In addition, numerical instability may become a problem with higher orders. However, the complexity of the LS algorithm is even slightly higher than that of the RLS algorithm [23].

The empirical CDFs for the ACPs and the time misalignments using the model reference control method in the presence of the adaptive predistorters are shown in Figs. 15 and 16, respectively. See the block diagram of the method shown in Fig. 6. The RF and envelope delays of the ET amplifier are random variables with uniform distribution between zero and one samples. The feedback delay is set to zero. The tunable delay block in the RF branch can be ignored because the linear predistorter takes care of the delays in the RF branch. The linear predistorter tries to drive the total delay in the RF branch towards 31 samples including the RF delay of the ET amplifier. The time misalignment is calculated assuming ideal timing of 31 samples which corresponds to the group delay of the transmitter, i.e. the same as the delay of the reference model block.

In the tracking phase, it is possible to increase the accuracy of the estimate by using a smaller step size in the cost function calculation. After the first iteration, the step size is reduced from 1 sample to 0.167 samples. After 10 iterations, the ACPs are almost all the time close to -60 dB and in addition, we achieve very accurate time misalignment estimations.

As discussed earlier, the adaptive linear predistorter takes care of all the delays in the RF and feedback branches and compensates them. Therefore, to achieve the complete time misalignment compensation, we can use the CCA method to estimate the delay in the envelope branch.

As can be seen in Figs. 17 and 18, the CCA method achieves also very good ACPs and time misalignment estimates. For instance, after 10 iterations, the absolute values of the time misalignments are all the time less than 0.01 samples and the ACPs are with 90 percent probability better than -60 dB. All the random delays are set just same as discussed above.

Finally, we assume that the adaptive linear predistorter cannot set the delay in the RF branch exactly to 31 samples, thus affecting the achievable ACPs in Fig. 17. The empirical CDF for the time misalignments using the CCA method, shown in Fig. 18, is calculated assuming ideal timing of 31 samples. For that reason, we cannot fairly compare the results shown in Fig. 18, because the total delay in the RF branch may not be exactly 31 samples due to inaccuracy of the linear predistorter. Therefore, to get more accurate timing estimates, we introduce an additional delay estimator, i.e. the VDP method, for the RF branch. The role of the VDP method is to estimate the residual RF + feedback delay, i.e. the delay after the compensation process of adaptive linear predistorter. In Fig. 17, we can see improved ACP performances. We notice that already after 5 iterations good performances are achieved, see the results for the CCA + VDP method in the figures.

Conclusion

In this work, we studied the nonideal ET amplifier. We proposed a general predistortion architecture and compared it to the state-of-the-art architecture. Using the considered architecture, we studied the performance of optimal and adaptive predistorters in terms of ACPs. In addition, we studied the compensation of the time misalignment between the RF and envelope signals in the ET amplifier. We proposed two methods to estimate and compensate the delays in the RF and envelope branches. We evaluated the performances of the methods in the presence of optimal as well as adaptive predistorters and compared them to the state-of-the-art method by analyses and simulations.

The results suggest that using the proposed architecture with the optimal predistorter, we achieve over 40 dB better ACPs than using a previously presented architecture. Moreover, adaptive nonlinear predistorter is a bottleneck for lower ACPs, at least with a reasonable order of polynomials, due to piecewise smoothness of amplitude and phase distortion behavior of the ET amplifier. In

addition, the studied time misalignment compensation methods give very accurate timing estimates. In the presence of optimal predistorter, the ACP loss compared to the input signal ACP is with 90 percent probability less than 10 dB. With adaptive predistorters, we cannot see any degradation of the ACP compared to the case of ideal timing.

References

[1] Kahn, L. R. (1952) Single-sideband transmission by envelope elimination and restoration. Proceedings of IRE, 40(7), 803–806.

[2] Saleh, A. A. M., Cox, D. C. (1983) Improving the power-added efficiency of FET amplifiers operating with varying-envelope signals. IEEE Transaction on Microwave Theory and Techniques, 31(1), 51–56.

[3] Sahu, B. Integrated, (2004) dynamically adaptive supplies for linear RF power amplifiers in portable applications. Ph.D. dissertation, Department of Electrical and Computer Engineering, Georgia Institute of Technology, Atlanta, GA.

[4] Wang, F., Yang, A. H., Kimball, D. F., Larson, L. E., Asbeck, P. M. (2005) Design of wide-bandwidth envelope-tracking power amplifiers for OFDM applications. IEEE Transaction on Microwave Theory and Techniques, 53(4), 1244–1255.

[5] Kaye, A. R., George, D. A., Eric, M. J. (1972) Analysis and compensation of bandpass nonlinearities for communications. IEEE Transaction on Communications, 20(10), 965–972.

[6] Woo, W. (2005) Hybrid digital/RF envelope predistortion linearization for high power amplifiers in wireless communication systems. Ph.D dissertation, Department of Electrical and Computer Engineering, Georgia Institute of Technology, Atlanta, GA.

[7] Raab, F. H. et al. (2002) Power amplifiers and transmitters for RF and microwave. IEEE Transaction on Microwave Theory and Techniques, 50(3), 814–826.

[8] Hekkala, A., Kotelba, A., Lasanen, M. (2008) Compensation of linear and nonlinear distortions in envelope tracking amplifiers. Proceedings of IEEE International Symposium on Personal, Indoor, and Mobile Radio Communications, Cannes, France, Sep. 15–18.

[9] Hekkala, A., Lasanen, M., Kotelba, A. (2008) Adaptive time misalignment compensation in envelope tracking amplifiers. Proceedings of IEEE International Symposium on Spread Spectrum Techniques and Applications, Bologna, Italy, Aug. 25–28.

[10] Kotelba, A., Hekkala, A., Lasanen, M. (2008) Compensation of time misalignment between input signals in envelope-tracking amplifiers. Proceedings of IEEE International Symposium on Personal, Indoor, and Mobile Radio Communications, Cannes, France, Sep. 15–18.

[11] Makundi, M., Valimaki, V., Laakso, T. I. (2001) Closed-form design of tunable fractional-delay allpass filter structures. Proceedings of IEEE International Symposium on Circuits and Systems, Sydney, Australia, May 6–9.

[12] Base Station (BS) Conformance Testing (FDD) (Release 5), 3GPP Technical Specification 25.141 version 5.8.0, 2003.

[13] Hussein, A. I., Kuhn, W. B. (2000) Bandpass SD modulator employing undersampling of RF signals for wireless communication. IEEE Transaction on Circuits and Systems II: Analog and Digital Signal Processing, 47(6), 614–620.
[14] Proakis, J. G., Manolakis, D. G. (1996) Digital Signal Processing: Principles, Algorithms, and Applications. Upper Saddle River, NJ: Prentice Hall, ch. 8.
[15] Widrow, B., Walach, E. (1996) Adaptive Inverse Control. Upper Saddle River, NJ: Prentice Hall, ch. 6.
[16] Lasanen, M., Kotelba, A., Hekkala, A., Järvensivu, P., Mämmelä, A. (2008) Adaptive predistortion architecture for nonideal radio transmitter. Proceedings on IEEE Vehicular Technology Conference Spring, Singapore, May 11–14.
[17] Ding, L. et al. (2004) A robust digital baseband predistorter constructed using memory polynomials. IEEE Transaction on Communications, 52(1), 159–165.
[18] Marsalek, R. (2003) Contribution to the power amplifier linearization using digital baseband adaptive predistortion. Ph.D. dissertation, Institute Gaspard Monge, University de Marne la Vallee, France.
[19] Widrow, B., Stearns, S. D. (1985) Adaptive Signal Processing. Englewood Cliffs, NJ: Prentice-Hall.
[20] Luenberger, D. (1989) Linear and Nonlinear Programming. Reading, MA: Addison-Wesley.
[21] Jacovitti, G., Scarano, G. (1993) Discrete time techniques for time delay estimation. IEEE Transaction on Signal Processing, 41(2), 525–533.
[22] Ding, L., Zhou, G. T. (2004) Effects of even-order nonlinear terms on power amplifier modeling and predistortion linearization. IEEE Transaction on Vehicular Technology, 53(1), 156–162.
[23] Proakis, J. G. (1995) Digital Communications. New York: McGraw-Hill.

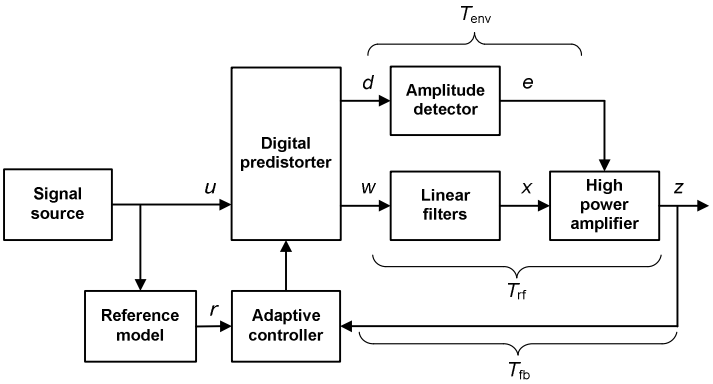

Fig. 1 Block diagram of the simplified system model

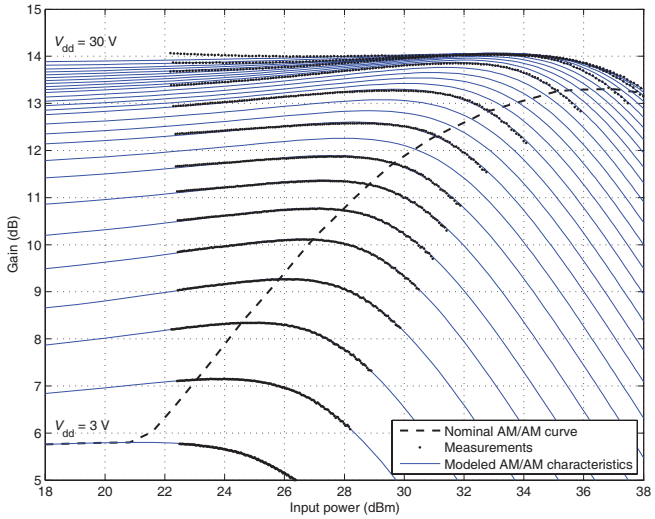

Fig. 2 ET amplifier gain as the function of input signal power level.

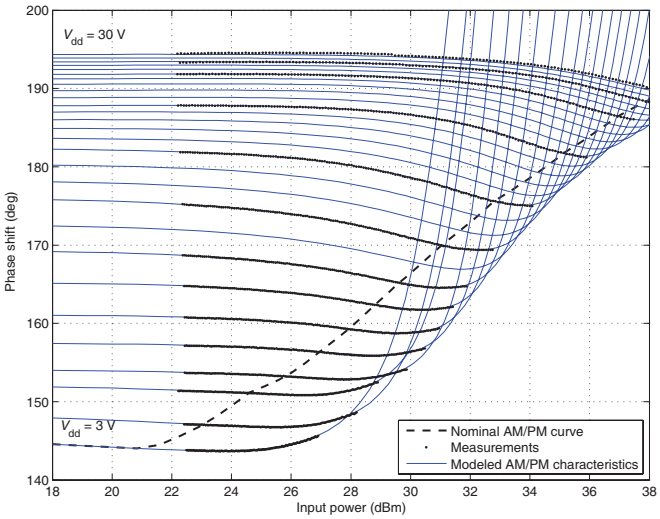

Fig. 3 Phase shift introduced by the ET amplifier as the function of input signal power level

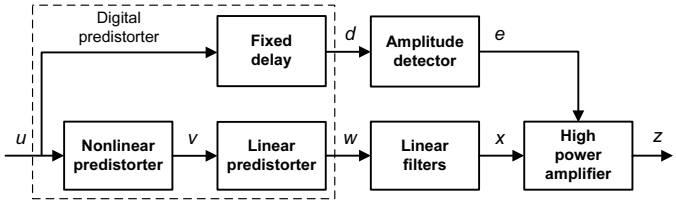

Fig. 4 Adaptive control structure with nonlinear predistorter only in RF branch

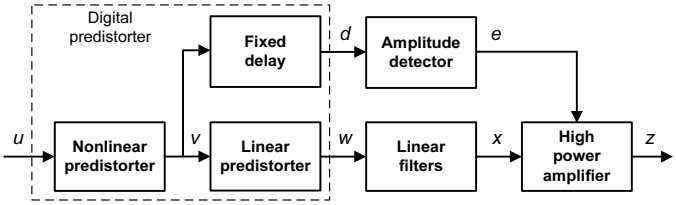

Fig. 5 Adaptive control structure with nonlinear predistorter in envelope and RF branches

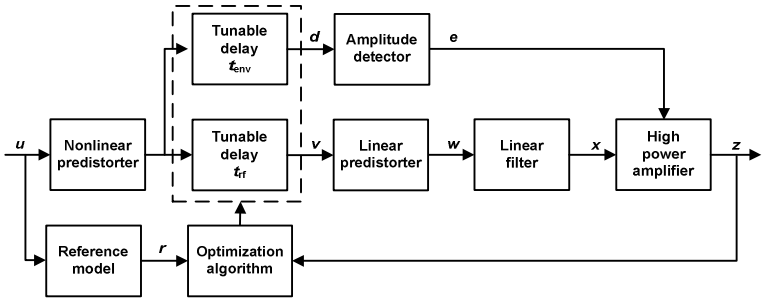

Fig. 6 Time misalignment compensation with a model reference structure

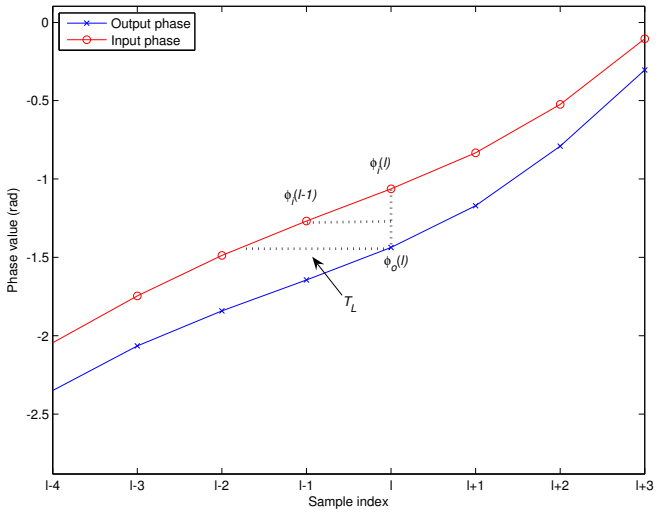

Fig. 7 Principle of the VDP calculation

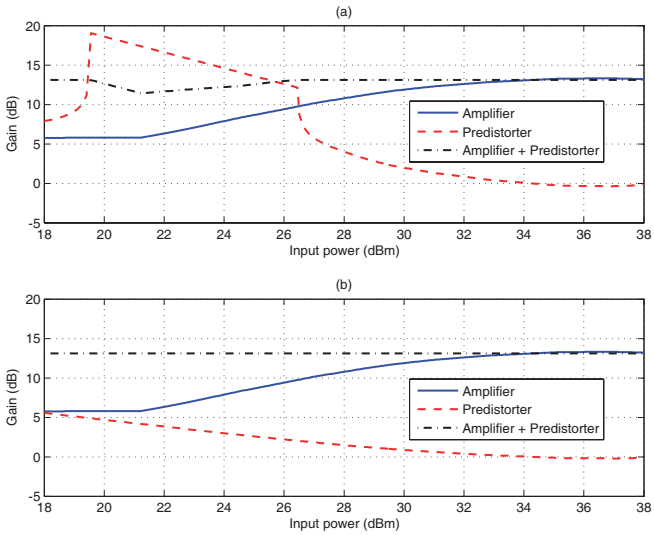

Fig. 8 AM/AM characteristics of amplifier and predistorter using the state-of-the-art (a) and the proposed (b) architectures

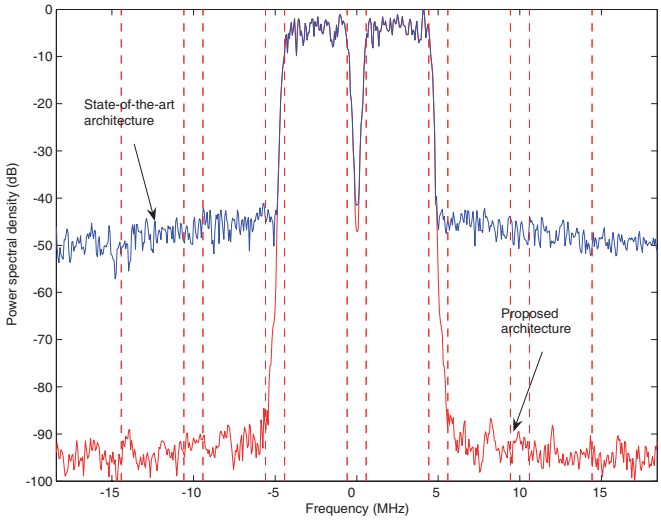

Fig. 9 Signal spectra at the output of predistorted HPA using the state-of-the-art and the proposed architectures

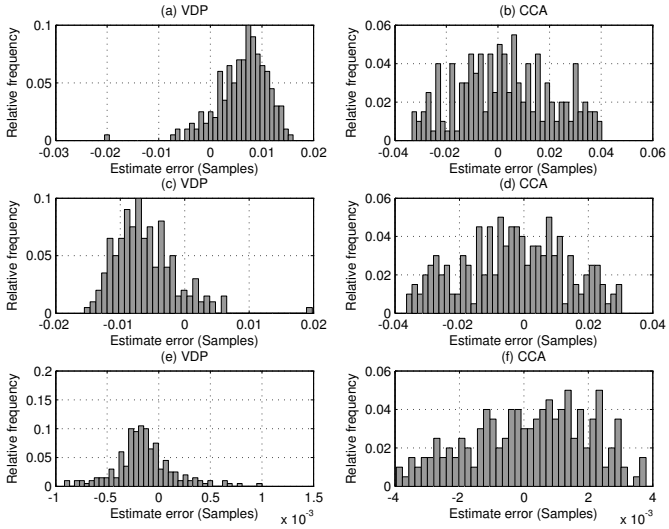

Fig. 10 Timing estimate error histograms using CCA and VDP methods after one in (a) and (b), two in (c) and (d), and three iterations in (e) and (f). feedback delay is 0 samples. Note the different scalings in the horizontal axes

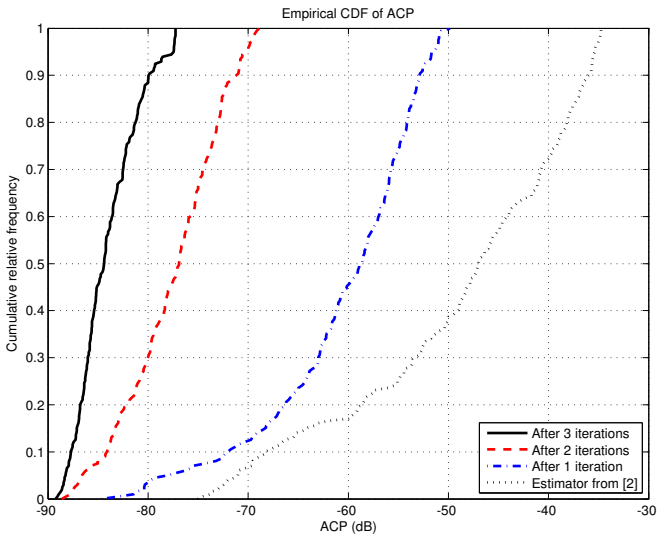

Fig. 11 Empirical CDFs of ACP using CCA and VDP methods after one, two, and three iterations. Results using estimator from [2] is plotted for comparison. feedback delay is 0 samples

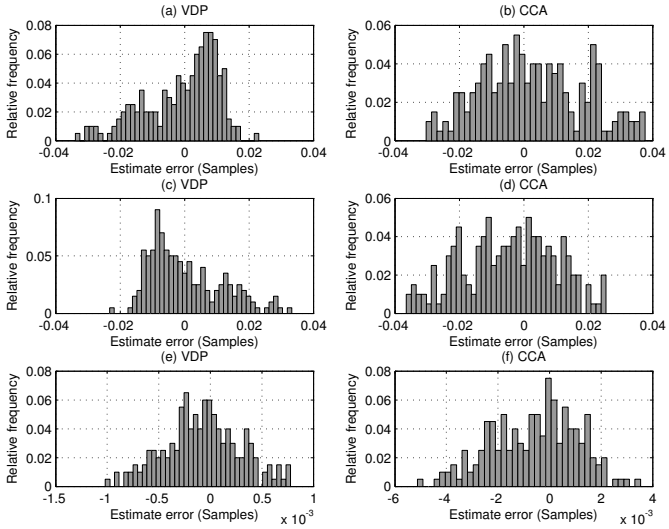

Fig. 12 Timing estimate error histograms using CCA and VDP methods after one in (a) and (b), two in (c) and (d), and three iterations in (e) and (f). feedback delay is 0.66 samples. Note the different scalings in the horizontal axes

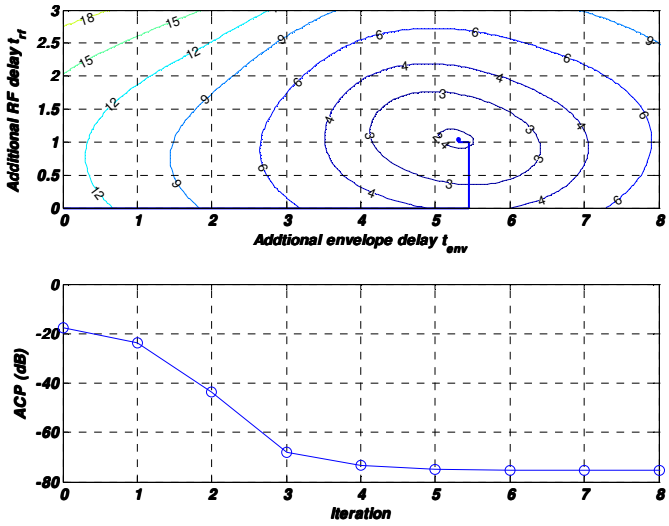

Fig. 13 Contour plot of the cost function $F(t_{\mathrm{env}}, t_{\mathrm{rf}})$ and achievable adjacent channel powers after subsequent iterations

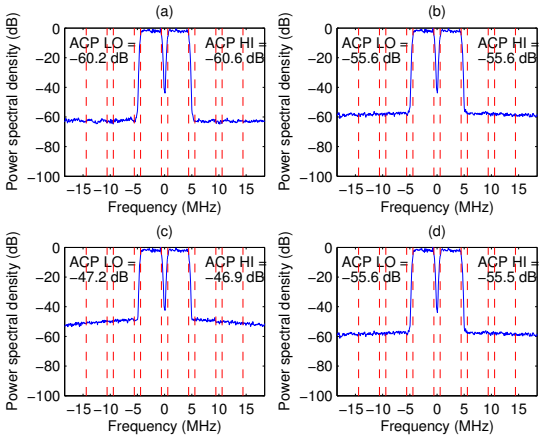

Fig. 14 ACPs at the output of HPA with linear and polynomial based nonlinear predistorters. (a) 9th order RLS, (b) 7th order RLS, (c) 5th order RLS, and (d) 7th order LS

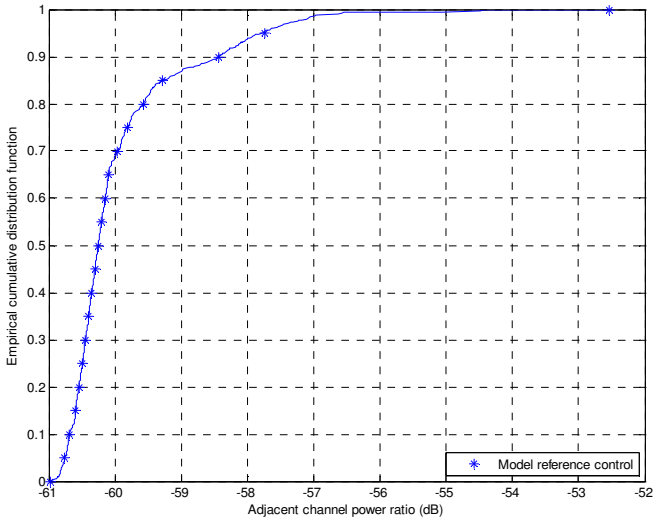

Fig. 15 Empirical ACPs after 10 iterations using model reference control method. Reduced step size in tracking mode

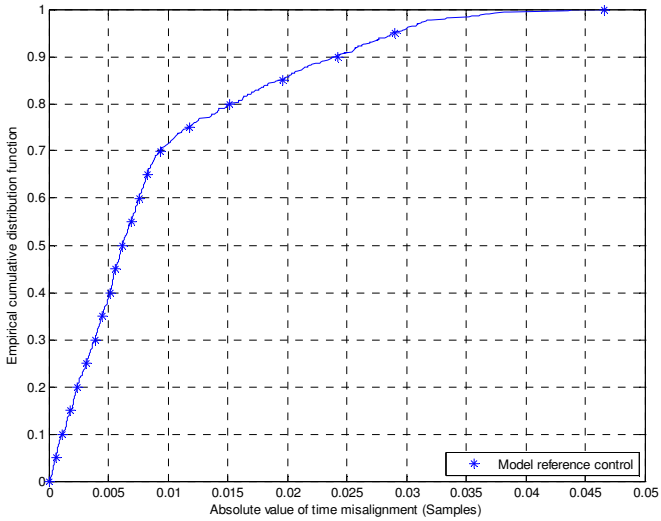

Fig. 16 Empirical time misalignments after 10 iterations using model reference control method. Reduced step size in tracking mode

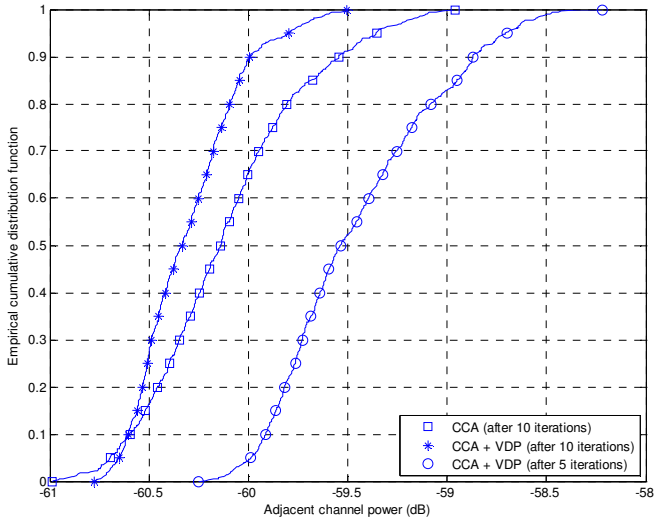

Fig. 17 Empirical ACPs using CCA and CCA + VDP methods

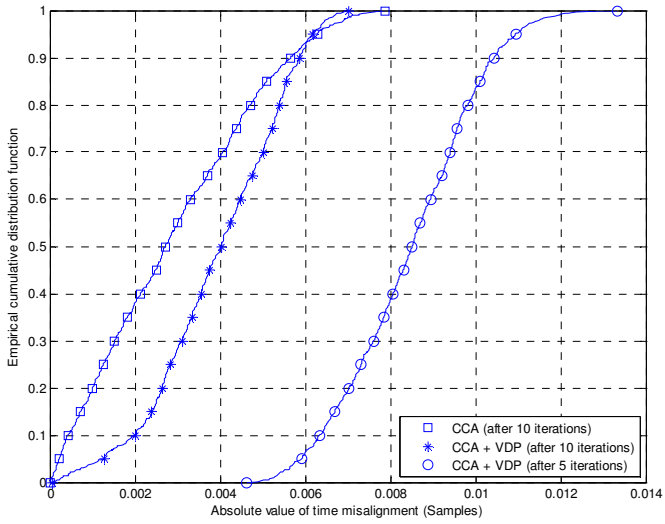

Fig. 18 Empirical time misalignments using CCA and CCA + VDP methods

Table 1 Parameters of envelope tracking amplifier model

V_s	g_0	g_1	L	a	b	p	q
3	1.890	0.147	1.917	0.141	1.292	0.673	–0.734
4	2.067	0.370	2.523	0.074	1.570	0.823	–0.655
5	2.301	0.486	3.126	0.034	1.931	0.926	–0.556
6	2.520	0.531	3.873	0.019	2.134	1.107	–0.511
7	2.793	0.530	4.569	0.018	2.011	1.252	–0.447
8	3.063	0.486	5.249	0.022	1.801	1.379	–0.389

9	3.333	0.441	5.967	0.028	1.537	1.496	–0.330
10	3.578	0.407	6.683	0.034	1.308	1.612	–0.276
12	3.913	0.373	8.058	0.035	1.063	1.835	–0.187
15	4.214	0.371	10.03	0.026	0.986	2.180	–0.086
20	4.465	0.338	13.38	0.014	0.908	2.760	0.023
25	4.673	0.233	16.46	0.008	0.701	3.488	0.104
28	4.807	0.146	18.27	0.006	0.577	4.011	0.134
30	4.945	0.066	19.48	0.005	0.560	4.080	0.168